



**HAL**  
open science

## Catalytic Production of Carbon Nanotubes by Fluidized-Bed CVD.

Régis Philippe, Aurore Morançais, Massimiliano Corrias, Brigitte Caussat,  
Yolande Kihn, Philippe Kalck, Dominique Plee, Patrice Gaillard, Daniel  
Bernard, Philippe Serp

► **To cite this version:**

Régis Philippe, Aurore Morançais, Massimiliano Corrias, Brigitte Caussat, Yolande Kihn, et al.. Catalytic Production of Carbon Nanotubes by Fluidized-Bed CVD.. Chemical Vapor Deposition, 2007, 1 (9), pp.447-457. 10.1002/cvde.200600036 . hal-03481270

**HAL Id: hal-03481270**

**<https://hal.science/hal-03481270v1>**

Submitted on 15 Dec 2021

**HAL** is a multi-disciplinary open access archive for the deposit and dissemination of scientific research documents, whether they are published or not. The documents may come from teaching and research institutions in France or abroad, or from public or private research centers.

L'archive ouverte pluridisciplinaire **HAL**, est destinée au dépôt et à la diffusion de documents scientifiques de niveau recherche, publiés ou non, émanant des établissements d'enseignement et de recherche français ou étrangers, des laboratoires publics ou privés.

DOI: 10.1002/cvde.200600036

Review

# Catalytic Production of Carbon Nanotubes by Fluidized-Bed CVD\*\*

By Régis Philippe, Aurore Morançais, Massimiliano Corrias, Brigitte Caussat, Yolande Kihn, Philippe Kalck, Dominique Plee, Patrice Gaillard, Daniel Bernard, and Philippe Serp\*

The large scale production of carbon nanotubes (CNTs) is a major issue for their use in industry. Among the different techniques used for their synthesis, catalytic (C)CVD in fluidized-bed reactors appears one of the most promising. In this article we present the current state of this new technology and we aim to highlight its great flexibility through examples which depict the selective preparation of different kinds of carbon nanomaterials from different catalysts. Finally, we present the results of scale-up experiments that permit an increase in carbon nanotube production by two orders of magnitude.

Keywords: Catalyst, CNTs, Fluidized-bed CVD, Graphite nanofibers

## 1. Introduction

Due to their outstanding electronic and mechanical properties coupled with their unique morphology, CNTs are currently identified as a fascinating material in nanotechnology. CNTs are expected to be included in a wide variety of applications and devices in the near future, and should bring significant breakthroughs in various fields such as engineering materials, energy, electronics, and ca-

alysis. Today, after almost two decades of intensive research, some innovations have already pushed CNTs from the laboratory to the commercial level, and an increasing number of industrial groups are turning their attention to adopting and incorporating CNTs in their products. Current commercial applications include motor vehicle fuel system components, flat panel displays, and specialized sports equipment. However, a number of issues, including high costs, standardization, safety and impact on the environment, and insufficient product yields in manufacturing, still need to be addressed. Additionally, further market penetration lies in the commercial success of CNT-based products in the open market.

As far as production processes are concerned, several techniques have been developed to produce CNTs in sizeable quantities. These include arc discharge, laser ablation, and CVD which are the more classic techniques, but CNTs can also be produced by ball-milling, diffusion flame synthesis, electrolysis, use of solar energy, heat treatment of a polymer, and low-temperature solid pyrolysis.<sup>[1]</sup> However, large-scale production of a consistently high quality material continues to be a serious challenge facing researchers. Among the processes mentioned above, CVD is now considered to be best for low-cost and large-scale synthesis of high-quality CNTs. An overview of CVD technologies has recently been reported.<sup>[2]</sup> Both plasma-enhanced (PE) and thermal heterogeneous (TH)CVD have been investigated to grow CNTs either on flat substrates or on catalyst powders. Both homogeneous and heterogeneous processes exist (Fig. 1).

[\*] Prof. P. Serp, Dr. R. Philippe, Dr. A. Morançais, Dr. M. Corrias, Prof. P. Kalck  
LCC/ENSIACET/INPT, UPR CNRS 8241  
118 route de Narbonne, 31077 Toulouse Cedex 4 (France)  
E-mail: Philippe.Serp@ensiacet.fr

Dr. R. Philippe, Dr. A. Morançais, Prof. B. Caussat  
LGC/ENSIACET/INPT, UMR CNRS 5503  
5 rue Paulin Talabot, BP1301, 31106 Toulouse Cedex 1 (France)

Dr. Y. Kihn  
CEMES, UPR CNRS 8011  
29 rue Jeanne Marvig, 31055 Toulouse (France)

Dr. D. Plee, Dr. P. Gaillard  
ARKEMA Lacq Research Center  
PO Box 34, 64170 Lacq (France)

Dr. D. Bernard  
ARKEMA  
4-8 cours Michelet, La Défense 10, F-92091  
Paris La Défense Cedex (France)

[\*\*] We thank Prof. Jean Pierre Couderc (LGC, Toulouse, France) for helpful discussions. Michel Molinier is gratefully acknowledged for his technical assistance in the design and manufacture of the FB-CVD reactors. These investigations were supported by Arkema Co., the French «Agence Nationale de Valorisation de la Recherche» (ANVAR) and the Conseil Régional de Midi-Pyrénées.

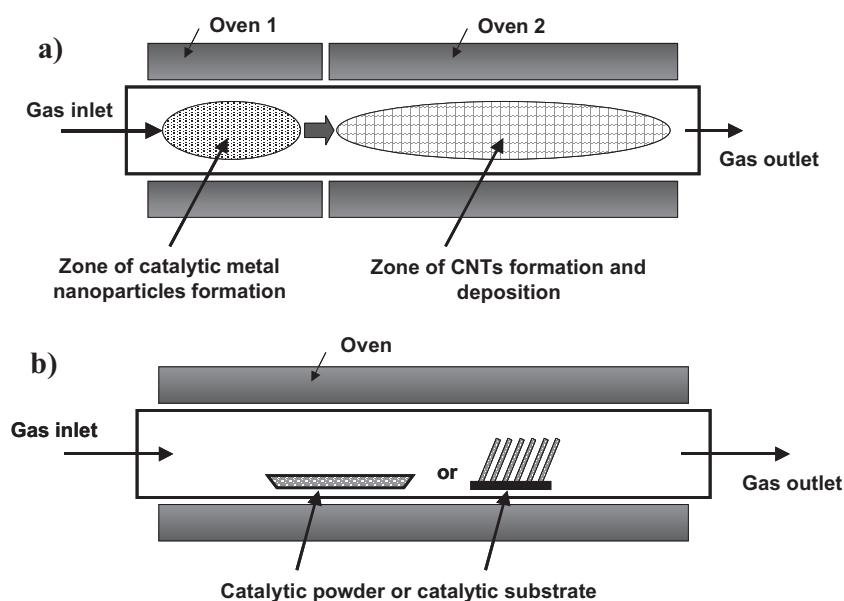


Fig. 1. Schematic representation of a) homogeneous and b) heterogeneous CVD processes for CNT growth.

The homogeneous CVD processes (Fig. 1a) are based on a homogeneous phase decomposition of two precursors, one for the metal and the other one for the carbon, and CNTs can be collected either on a substrate or as a powder in, or at, the exit of the CVD reactor. These processes suffer two main drawbacks; i) the difficulty of controlling the size of the metal catalyst nanoparticles due to the high temperatures required, and to the thermal profile of the reactors which may induce poor selectivity towards CNT production, and ii) the possibility of reactor plugging due to carbon deposition in the CVD reactor. Heterogeneous processes (Fig. 1b) consist of the decomposition of certain hydrocarbons on small metal particles, or thin films deposited on a substrate. In the case of flat substrates, aligned CNTs can be produced for specific applications such as flat panel displays, whereas when powders are used to support the catalyst particles, CNTs are usually produced as three dimensional, randomly oriented hanks in which the grains of the heterogeneous catalyst are embedded.



*Philippe Serp has been Professor of Inorganic Chemistry at the Ecole Nationale Supérieure des Ingénieurs en Arts Chimiques Et Technologique in Toulouse University since 2005. After receiving his Ph.D. (with P. Kalck) in 1994 from the Université Paul Sabatier in Toulouse where he worked on CVD catalysts, he moved to Universidade de Porto (Portugal) to carry out postdoctoral research (with J.L. Figueiredo) on catalytic CVD to prepare carbon filaments, and to the Université Catholique de Louvain-la-Neuve in Belgium (with J.P. Issi) where he worked on the characterization of catalytic carbon filaments. He was the recipient of the Catalysis Division of the French Chemical Society Award in 2004, and the APDF « Celestino da Costa/Jean Perrin » award in 2005.*

*His current research interests in Laboratoire de Chimie de Coordination include CVD and catalytic CVD preparation of nanostructured materials as nanoparticles, nanotubes, or nanowires, and the understanding of homogeneous catalytic reactions, fields in which with co-workers he has published over 80 papers, including 6 review articles, 8 book chapters and 8 patents.*

When using heterogeneous powder catalysts, horizontal and vertical hot-wall CVD reactors have been used. In the most common technology, the catalyst powder is poured into a quartz or alumina boat which is set at the center of a horizontal CVD reactor.<sup>[2]</sup> Alternatively, CVD reactors based on a rotary kiln have been used for large-scale production, and in this case, no quartz or alumina boat is required.<sup>[3]</sup> For vertical reactors, fixed or fluidized beds of catalysts have been used. The efficiency of CNT growth in most of these processes (use of quartz or alumina boats, rotary kiln, and fixed bed) is severely limited by inhomogeneous gas/solid contacts and temperature gradients. However, for fluidized-bed (FB)-CVD, as an intense mixing of solids is ensured by the gas flow, optimal process conditions can be found, allowing high carbon conversions and a selective catalytic formation of CNTs. Thus, it

appears that this technique is currently the most promising one for a large-scale production of CNTs of a consistently high quality.

In this article we will first review catalytic CNT production using the FB-CVD technology, and then detail the results, including scale-up experiments, obtained in our laboratories for CNT production by FB-CVD on supported catalysts.

## 2. Current State of Catalytic CNT Production by FB-CVD

In the production of CNTs, the FB-CVD technique offers numerous advantages such as an optimized gas/solid contact compared to fixed bed reactors, and the absence of any thermal gradient so that optimal mass and heat transfer are reached in the reaction zone.<sup>[4]</sup> This is also a flexible process in terms of operating conditions, and parameters

such as catalytic composition, gas mixture, and temperature can be finely tuned according to the definition of the desired product. Additionally, it offers the possibility of working in either batch or continuous mode. All these characteristics allow a homogeneous and selective production of carbon nanomaterials, so this process should be attractive for production on the industrial scale. It is also worth noting that the fluidized-bed technology is currently used and well-controlled for classic industrial catalytic processes such as polyethylene manufacture<sup>[4]</sup> or catalytic cracking of hydrocarbons.<sup>[5]</sup>

The first studies dealing with FB-CVD for multi-wall (MW)CNT or graphite nanofiber (GNF) production appeared in the early 2000 s, and more recently, this technique has also been used for the synthesis of single-wall (SW)CNTs. An important fact highlighting the potential of this technology is that pilot industrial FB-CVD reactors for the production of MWCNT and SWCNT manufacture are already running. Indeed, Arkema commercializes MWCNTs named Graphistrength™, and SouthWest Nanotechnologies produce SWCNTs by the CoMoCAT™ meth-

od which uses this technology. Due to the large diversity of operating conditions, particularly CVD run duration, gas flow composition, temperature, and catalysts used, and in order to be able to compare the results obtained in the different studies reported in the open literature<sup>[4-29]</sup> we have chosen to focus on two parameters; the productivity  $X$  ( $g_{CNT}/g_{cata}$ ) and the catalytic activity  $A$  ( $g_{CNT}/g_{active\ phase}/h$ ). We will also try to highlight tendencies concerning the catalytic systems, the operating conditions, and the resulting nanomaterials. The main results reported in these studies are presented in Table 1 in terms of productivity, activity, and selectivity (type of CNT).

Several catalytic systems, mainly based on iron, cobalt, and nickel have been used to grow CNTs by FB-CVD. Nickel is preferred for the growing of GNFs due, in particular, to its tendency to form the faceted nanoparticles necessary for the epitaxial growth of the graphene layers in GNF. Bimetallic catalysts based on Fe and Co in association with molybdenum, or less often with tungsten, can be used to grow SWCNTs. The role of the second metal is to dilute the active Fe or Co phase by forming a mixed oxide

Table 1. Selected examples of catalytic production of CNTs by FB-CVD. (ns = not specified)

Catalyst	Metal loading [% w/w]	Preparation method	Gas phase	$T$ [°C]	Product	$X$ [ $g_{CNT}/g_{cata}$ ]	$A$ [ $g_{CNT}/g_{Metal\ h^{-1}}$ ]	Ref.
Fe/SiO <sub>2</sub>	<5	CVD	C <sub>2</sub> H <sub>4</sub> , H <sub>2</sub> , N <sub>2</sub>	650	MWCNTs	0.05	1	4
Co/La <sub>2</sub> O <sub>3</sub>	25	Impregnation	C <sub>2</sub> H <sub>2</sub> , H <sub>2</sub>	700	MWCNTs	27.9	55.6	5
Ni/Al <sub>2</sub> O <sub>3</sub>	90	Co-precipitation	CH <sub>4</sub> , N <sub>2</sub>	550	GNFs	145	11.1	6
Co-Mo/SiO <sub>2</sub>	0.5–1.5	Impregnation	CO	ns <sup>a</sup>	SWCNTs	ns	?	7
Ni/SiO <sub>2</sub>	30 to 96	Co-precipitation	CH <sub>4</sub> , N <sub>2</sub>	550	GNFs	300	10.4	8
Fe/Al <sub>2</sub> O <sub>3</sub>			Pentane or					
Ni/zeolite	ns	Coating	octene	600–1000	MWCNTs	ns	?	9
Fe <sub>2</sub> O <sub>3</sub> /MgO	2.5 to 15	Impregnation	C <sub>2</sub> H <sub>2</sub> or CH <sub>4</sub> , H <sub>2</sub> , N <sub>2</sub>	450–800	MWCNTs	0.54	10.8	10
LaCoO <sub>3</sub>	25	Impregnation	CH <sub>4</sub> , H <sub>2</sub> , N <sub>2</sub>	700	MWCNTs	22	44.0	11
LaFeO <sub>3</sub>	ns	Impregnation	CH <sub>4</sub> , H <sub>2</sub> , N <sub>2</sub>	980	MWCNTs	ns	ns	12
Fe/Al <sub>2</sub> O <sub>3</sub> , SiO <sub>2</sub> , TiO <sub>2</sub> or ZrO <sub>2</sub>	max 85	Sol-gel	CH <sub>4</sub> , H <sub>2</sub>	650–800	MWCNTs and GNFs	13.5–45	ns	13
Fe/SiO <sub>2</sub>	2.5 to 29	Sol-gel	C <sub>2</sub> H <sub>2</sub> , H <sub>2</sub> , N <sub>2</sub>	700	MWCNTs and GNFs	0.11	0.4	14
Fe/Al <sub>2</sub> O <sub>3</sub>	ns	Co-precipitation	C <sub>2</sub> H <sub>4</sub> , H <sub>2</sub> , N <sub>2</sub>	550	MWCNTs	20	ns	15
Ni/SiO <sub>2</sub>	0.7 to 60	Impregnation	CH <sub>4</sub> , Ar	760	SWCNTs, GNFs, encapsulated NPs	0.15	0.75	16
								36
Fe-Ni/Al <sub>2</sub> O <sub>3</sub>	45–5	Co-precipitation	CH <sub>4</sub> , N <sub>2</sub>	550	GNF, MWCNT	14.5	14.5	17
Fe/SiO <sub>2</sub> or Al <sub>2</sub> O <sub>3</sub>	ns	ns	Propylene, N <sub>2</sub>	600	MWCNT	4	ns	18
Fe-Mo/Al <sub>2</sub> O <sub>3</sub>	60–6	Co-precipitation	LPG	650	MWCNT	8	4.0	19
Ni-Cu/Al <sub>2</sub> O <sub>3</sub>	ns	ns	CH <sub>4</sub> , H <sub>2</sub> , N <sub>2</sub>	850	GNF, MWCNT	ns	ns	20
Fe/Al <sub>2</sub> O <sub>3</sub>	ns	ns	C <sub>2</sub> H <sub>4</sub> , H <sub>2</sub> , N <sub>2</sub>	500–700	MWCNT	1–20	ns	21
Fe/Al <sub>2</sub> O <sub>3</sub>	2.5	CVD	C <sub>2</sub> H <sub>4</sub> , H <sub>2</sub> , N <sub>2</sub>	650	MWCNT	0.27	5.4	22
Co/MgO	56	ns	CO, N <sub>2</sub> , H <sub>2</sub>					
CuNi	80	ns	C <sub>2</sub> H <sub>4</sub> , N <sub>2</sub> , H <sub>2</sub>	500–700	CNT, GNF	ns	ns	23
Fe-Mo or W/MgO	10–3	Impregnation	CH <sub>4</sub> , Ar, H <sub>2</sub> O	1000	SWCNT	0.52	ns	24
Fe/MgO	?	Impregnation	CH <sub>4</sub> , Ar	850	SWCNT	0.55	ns	25
Ni/MgO	50	ns	CH <sub>4</sub>	580	GNF	10	20	26
ns	ns	ns	N <sub>2</sub> , C <sub>2</sub> H <sub>2</sub>	750	MWCNT	ns	ns	27
Fe-Mo/MgO	ns	Co-precipitation	Ethanol, Ar	ns	SWCNT	ns	ns	28
Al <sub>2</sub> O <sub>3</sub>	ns	–	Polyolefin, N <sub>2</sub>	450–850	MWCNT	ns	ns	29

phase that produces very small and active particles during the very early steps of the growth process. The support also takes an important part in the catalyst since it should; i) allow a convenient interaction with the metal and then a good dispersion of the metallic phase, ii) be easily removed after the growth process in order to get pure CNTs, and iii) be conveniently fluidized. Classic oxides, such as SiO<sub>2</sub>, Al<sub>2</sub>O<sub>3</sub>, MgO, TiO<sub>2</sub>, ZrO<sub>2</sub>, zeolites or perovskites have been used as supports in heterogeneous catalysis for CNT growth. Silica and alumina are the most common supports since they develop high surface area and high mesoporosities that permit the production of well-dispersed supported catalysts. Moreover, these supports generally belong to groups A or B of Geldart's classification and are easily fluidized.<sup>[4]</sup> Magnesia is used because of its easy dissolution in diluted mineral acids, but often suffers from poor fluidization (cohesive powders from group C of Geldart's classification). Zeolites offer the possibility of nanoparticles being confined in their cages (template effect), and titanium dioxide is well known for its strong metal-support interaction properties that can allow the production of well-dispersed nanoparticles even at the high temperatures required for these CVD processes. The synthetic procedures used to produce the supported metal catalysts necessary for CNT growth are among the most common in heterogeneous catalysis; liquid impregnation, co-precipitation, or sol-gel. The metal loading may change significantly from a few wt.-% to the quasi-totality of the catalyst (for instance 96 % for a Ni/SiO<sub>2</sub> catalyst).<sup>[10]</sup> Low loadings are generally used for SWCNT growth where very small nanoparticles (1–5 nm) are required at high temperatures, whereas high loadings are used for GNF growth.

The operating conditions used for CNT growth show less flexibility. In general, the gas phase contains; i) an inert carrier gas such as nitrogen or argon, argon being preferred for SWCNT growth, to dilute the carbon source and reach a fluidization regime, ii) hydrogen, present to prevent poisoning of the catalytic surface by carbon deposition, and iii) the carbon source. The choice of this latter has a significant influence on the temperature of the CVD process and thus on the type of CNT produced. Carbon monoxide or methane are used for SWCNT growth between 800 and 1000 °C; ethylene or acetylene are decomposed at lower temperatures, between 600 and 800 °C, to grow MWCNTs, and GNFs can be produced at still lower temperatures (<600 °C) from methane. Other carbon sources such as n-pentane,<sup>[11]</sup> propene,<sup>[20]</sup> or LPG,<sup>[21]</sup> have also been used. Ethanol<sup>[30]</sup> may also be convenient since its decomposition produces hydroxyl radicals that may clean the surface of the produced CNTs during the CVD process. Finally, a recent study<sup>[31]</sup> reports the use of plastics (virgin or recycled polyethylene) to grow CNTs in a fluidized-bed reactor.

General trends appear concerning the catalytic FB-CVD growth of CNTs. It seems that, independent of the support, the metal, or the carbon source; i) the highly loaded cata-

lysts prepared by co-precipitation produce mainly GNFs with a high productivity and a moderate activity, or MWCNTs with poor selectivity, ii) MWCNTs can be produced with high selectivity on catalysts characterized by moderate loadings (2.5–15 % w/w) with both good productivity and high activity, and iii) SWCNTs production requires low metal loadings (generally <2.5 % w/w) with, however, a low productivity, that means that the characteristics of the powder (diameter, density) do not change significantly during the CVD operations. It is worth noting that these tendencies are not specific to FB-CVD but to CCVD on supported catalysts.

In addition, for FB processes the temporal evolution, during runs, of some physical characteristics of the catalytic powder and of the composite catalyst/CNT powder must be taken into account since these parameters have a direct influence on the quality of the fluidization and thus on the gas/solid contact, on the temperature profile, and finally on the quality of the carbon materials. Additionally, when operating in FB-CVD, some constraints originate from; i) imposed CVD conditions, ii) side deposition on the reactor walls and on the gas distributor, iii) eventual clogging of the bed due to high deposition rates and/or to low fluidization quality, and iv) homogeneous nucleation.<sup>[32]</sup> Unfortunately, these fundamental aspects of the FB-CVD process have been almost systematically occulted in the studies presented in Table 1. Thus, it is impossible to evaluate and compare the hydrodynamic behavior of the bed during these syntheses. Only Wei and co-workers<sup>[17,21,23,33]</sup> and Corrias et al.<sup>[24]</sup> present, in the case of MWCNT growth, some data on size and density evolution of the composite powders during the synthesis, and report important bed expansions during the CVD process. Thus, the main peculiarity of this process compared to other FB-CVD processes,<sup>[32]</sup> is the dynamic and significant evolution of the composite powder during the CVD operation. Indeed, due to the unique morphology of MWCNTs (huge aspect ratio), the original catalytic powder, if very active (e.g., Fe/Al<sub>2</sub>O<sub>3</sub>) is rapidly covered by a dense network of MWCNTs.<sup>[24,33]</sup> The diameter of these agglomerates increases with run duration whereas their density decreases significantly and these two factors lead to high bed expansions. This phenomenon has to be taken into account in the design of any FB-CVD reactor. If the catalyst used for MWCNT growth presents a low activity, as Fe/SiO<sub>2</sub>,<sup>[6,16]</sup> the diameter of the grains and their density will be less affected. Important bed expansions may be a serious drawback for industrialization since large volume reactors will be needed. However, a recent study has shown that this phenomenon can be significantly reduced by a slight increase in the operating temperature,<sup>[24]</sup> allowing the formation of more compact agglomerates. It is worth noting that this phenomenon should be much less pronounced for SWCNT growth since low activities are generally measured, whereas it should be taken into account for GNF synthesis as the productivities could be very high ( $X > 100 \text{ g}_{\text{GNF}}/\text{g}_{\text{cata}}$ ).

If we consider the FB-CVD reactor design, three types of fluidized-bed reactors have been used (Fig. 2). The most usual and the simplest one<sup>[17]</sup> consists of a fluidization column heated with an electric oven, and equipped with a distributing plate to support the fluidized catalyst powder (Fig. 2a). The gas flow crosses the fluidized bed, and filters are installed at the exit of the reactor to collect fine particles. The reactor outlet can be equipped with a cyclone to minimize fine particles being carried away. A gas chromatograph may also be conveniently sited at the reactor outlet to determine online the gas-phase composition during the synthesis. Possible improvements consist in setting an additional oven before the fluidized bed in order to pre-heat the gas (Fig. 2b),<sup>[22]</sup> or to install a vibration system<sup>[8]</sup> (vibro-fluidized-bed reactor, Fig. 2c), in order to improve the fluidity of beds by breaking channels and cracks. Although most of the studies deal with small-diameter reactors (i.d. <3 cm), recent studies report the use of larger FB-CVD reactors (i.d. >10 cm) in which the effects of the walls are minimized.<sup>[23]</sup> Furthermore, as already stated above, some companies, such as Arkema and SouthWest Nanotechnologies, have already built pilot industrial reactors using this technology. Even if data concerning the scale-up process are not available in the open literature, the existence of these reactors shows the feasibility of this operation.

### 3. Catalytic Production of GNFs and MWCNTs by FB-CVD, and Scale-Up Operations

Some years ago, we initiated a research program devoted to CNT manufacture by FB-CVD, in a joint project associating chemists from catalysis and chemical engineers. In this section we want to highlight the flexibility of this technology, which allows the production of various kinds of CNTs, namely GNFs or MWCNTs, just by changing the metal used for catalysis, while keeping the same, easily available carbon source, ethylene, and the same FB-CVD

reactor. Additionally, we will present some results concerning the scale-up operation which has led to an increase of two orders of magnitude in MWCNT production.

#### 3.1. Catalytic Production of GNFs and MWCNTs by FB-CVD

##### 3.1.1. FB-CVD Synthesis of GNFs on a Ni/Al<sub>2</sub>O<sub>3</sub> Catalyst

The influence of temperature on the synthesis of GNFs from ethylene on a Ni/Al<sub>2</sub>O<sub>3</sub> catalyst was investigated for the range 400–750 °C. The results are presented in Table 2 and Figure 3. We observe that the catalyst productivity increases between 400 °C and 500 °C and then remains constant from 500 to 750 °C. The activity of the catalyst also shows two distinct zones; i) between 400 °C and 500 °C, where the catalytic activity increases, following an Arrhenius-type law, with an activation energy of 162 kJ mol<sup>-1</sup> (consistent with the activation energy of 145 kJ mol<sup>-1</sup> for carbon diffusion through nickel<sup>[35]</sup>), and ii) a second between 500 °C and 750 °C, where the activity is quite constant, with a slight decrease that we can relate to catalyst deactivation (negative energy of activation). This non-Arrhenius temperature dependence at high temperatures for nickel-supported catalysts has already been reported.<sup>[36–38]</sup> All the authors attribute the deactivation process to the relationship existing between the reduction temperature, the synthesis temperature, and the nickel particle sizes. Indeed, small particles lead to higher growth rates but also to higher deactivation rates. Many results suggest that deactivation is due to pyrolytic carbon formation when the overall reaction is too fast. This carbon encapsulates the active metal particles and leads to the end of GNF growth. This pyrolytic carbon formation is a consequence of the difference existing between the rate of decomposition of the carbon source and the carbon diffusion rate through the particle. At high temperatures, the decomposition rate is too

fast and carbon precipitation occurs simultaneously with GNF growth because of the too high carbon supply.

In our case, if we consider the diameters of the GNFs, measured using transmission electron microscopy (TEM) observations, higher temperatures lead to smaller GNF diameters and thus to smaller nickel particles, observations that fit well with the experimental results. TEM analyses (Fig. 4) show that, at each temperature, the deposited GNFs are homogeneous in diameter and that there is no additional product. We can link the good selectivity with the good isothermal profile of the catalytic bed in this FB-CVD contacting process. Ad-

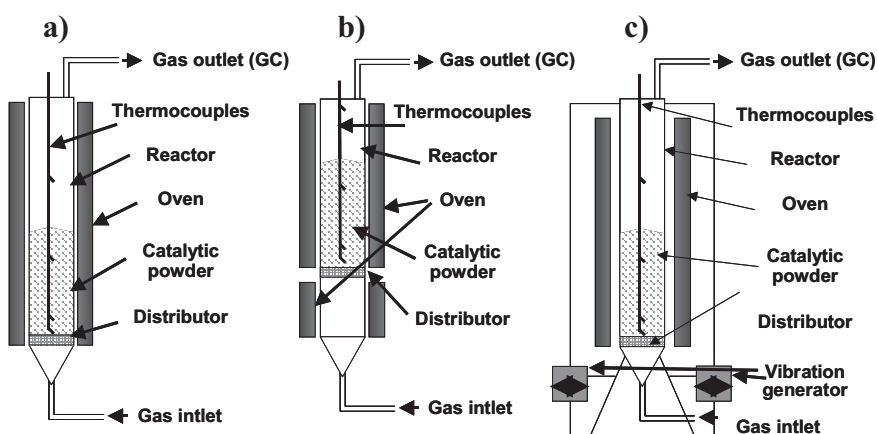
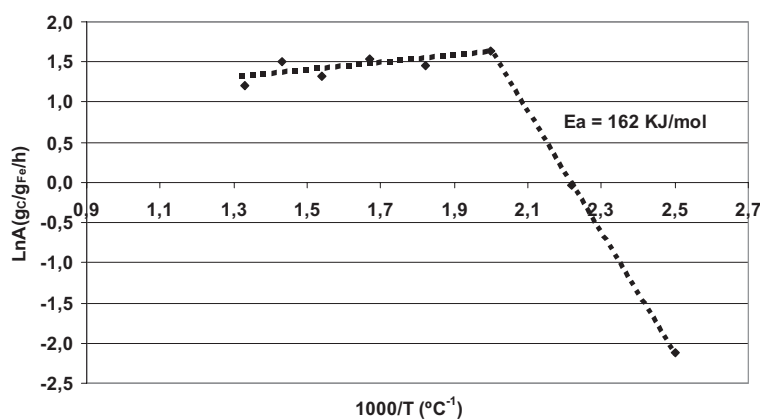


Fig. 2. Types of FB-CVD reactor for CNT synthesis: a) standard configuration, b) with gas pre-heating, and c) vibro-fluidized-bed reactor.

Table 2. Operating conditions and results obtained for Ni/Al<sub>2</sub>O<sub>3</sub> catalysts.

T [°C]	Q <sub>C<sub>2</sub>H<sub>4</sub></sub> [sccm]	Q <sub>N<sub>2</sub></sub> [sccm]	Q <sub>H<sub>2</sub></sub> [sccm]	Final fixed bed height [cm]	Ethylene conversion [%]	X [gC/g <sub>cata</sub> ]	A [gC/g <sub>M</sub> h <sup>-1</sup> ]
400				~0.1	0.14	0.01	0.12
450				~0.15	1.11	0.08	0.96
500				0.4	5.91	0.43	5.12
550				0.35	4.94	0.36	4.29
600	60	160	120	0.4	5.33	0.38	4.63
650				0.3	4.33	0.31	3.76
700				0.4	5.17	0.37	4.48
750				0.3	3.86	0.28	3.35


 Fig. 3. Arrhenius plot for activation energy of GNF growth on Ni/Al<sub>2</sub>O<sub>3</sub> catalysts.

ditionally an important fact is that the synthesis temperature has a strong influence on the external diameters of the resulting GNFs. Indeed, between 400 and 500 °C, the mean diameters are in the range 50–60 nm, and between 550 and 750 °C, the mean diameter falls in the range 10–20 nm. As

already stated, we explain this by the peculiar temperature dependence of the structural changes in the nickel active particles occurring during the reductive heating-up process. As the angle between the graphene layers of GNFs and the fiber axis is not affected by the temperature and remains near 20°, we believe that a similar “epitaxial growth” of carbon on the faces of nickel particles operates between 400 and 750 °C. Thus the structural changes of Ni particles should concern mainly their mean particle size.

On the macroscopic scale, when GNF deposition occurs, we can observe an increase in the bed height which is proportional to the productivity. At 500 °C, where the highest productivity is achieved, the fixed-bed height is roughly four times more important than in the initial case. Scanning electron microscopy (SEM) analysis for the experiment conducted at 650 °C (Fig. 5) shows that GNF production leads to the explosion of the catalyst grains and to a very homogeneous coverage of the catalyst surface. This explosion has been confirmed by laser granulometry analysis (Fig. 6) performed on the catalyst before and after synthesis, after air calcination of the carbonaceous products. All these observations suggest that carbon deposition occurs first on the surface of the catalytic grains and then in the mesopores of the catalyst, leading to grain explosion and continuation of GNF growth, thus

ensuring an homogeneous coverage of the pieces formed. This phenomenon is responsible for the bed expansions, with a decrease of the apparent grain density due to GNF formation. This leads to an increase of the ( $U/U_{mf}$ ) ratio and explains why very small initial bed heights and low initial ( $U/U_{mf}$ ) ratios have been selected.

Finally, the Raman spectrum (Fig. 7a) of the purified GNFs synthesized at 650 °C shows the D and G peaks characteristic of disordered carbon and graphite, respectively. The  $I_D/I_G$  ratio of 0.92 is consistent with graphitic GNF.<sup>[40]</sup> Conducted after purification, the thermogravimetric analysis (TGA) showed a purity of 95% (5% of remaining nickel), while the Brunauer-Emmett-Teller (BET) measurements showed a surface area of 167 m<sup>2</sup> g<sup>-1</sup> with a pore volume of 0.50 mL g<sup>-1</sup>.

### 3.1.2. FB-CVD Synthesis of MWCNTs on a Fe/Al<sub>2</sub>O<sub>3</sub> Catalyst

To show the flexibility of the FB-CVD process, we also investigated

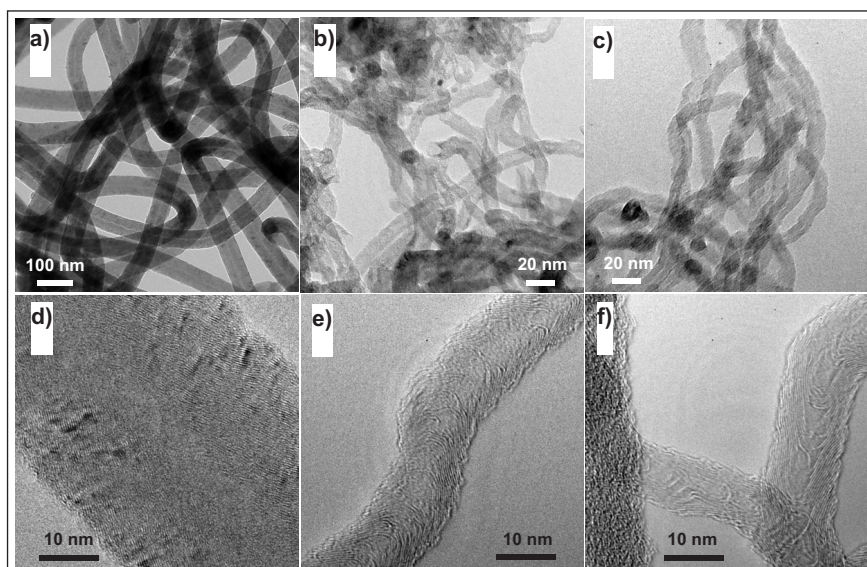


Fig. 4. TEM images of GNFs grown at a) and d) 550 °C, b) and e) 650 °C, and c) and f) 750 °C.

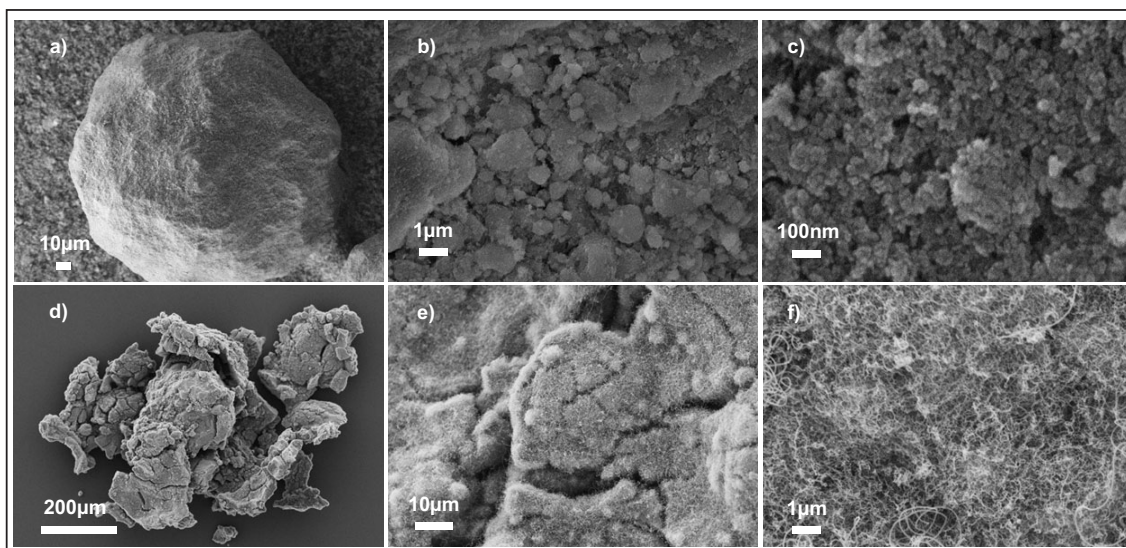


Fig. 5. SEM images of the Ni catalyst and the composite powder obtained at 650 °C: a–c), original Ni/Al<sub>2</sub>O<sub>3</sub> catalyst, and d–f), composite powder.

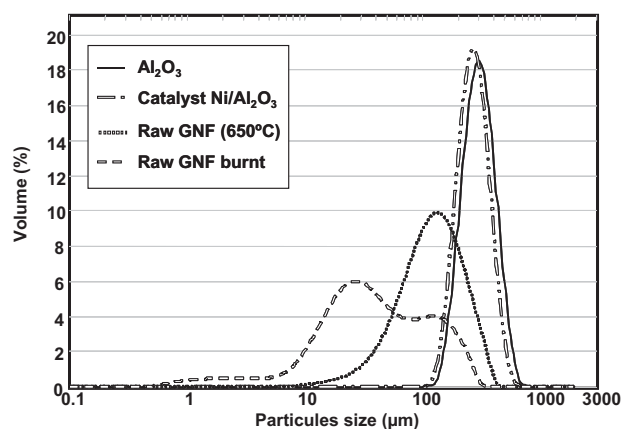


Fig. 6. Laser granulometry analysis of powders involved in the nickel-catalyzed FB-CVD process.

the influence of temperature on the synthesis of MWCNTs from ethylene on Fe/Al<sub>2</sub>O<sub>3</sub> catalysts between 550 °C and 750 °C, as detailed in Table 3 (runs 2-1 to 2-6). Results are presented in Table 4 and Figure 8. It is worth noting that a partial bed agglomeration occurred near the distributor for runs reaching the highest productivities. We observe that the productivity and the catalytic activity increase between 550 °C and 650 °C, where they reach a maximum before starting to decrease above 650 °C. Both these behaviors fit well with Arrhenius-type laws with, respectively, an activation energy of 57 kJ mol<sup>-1</sup> and a negative activation energy due to catalyst deactivation. This value of 57 kJ mol<sup>-1</sup> is in good agreement with that obtained by Baker et al. for carbon diffusion through  $\alpha$ -iron.<sup>[35]</sup> The deactivation observed at high temperatures for the present iron catalysts seems to be in the same range as for nickel catalysts ( $E_d = -7$  kJ mol<sup>-1</sup>). This deactivation is related to the differ-

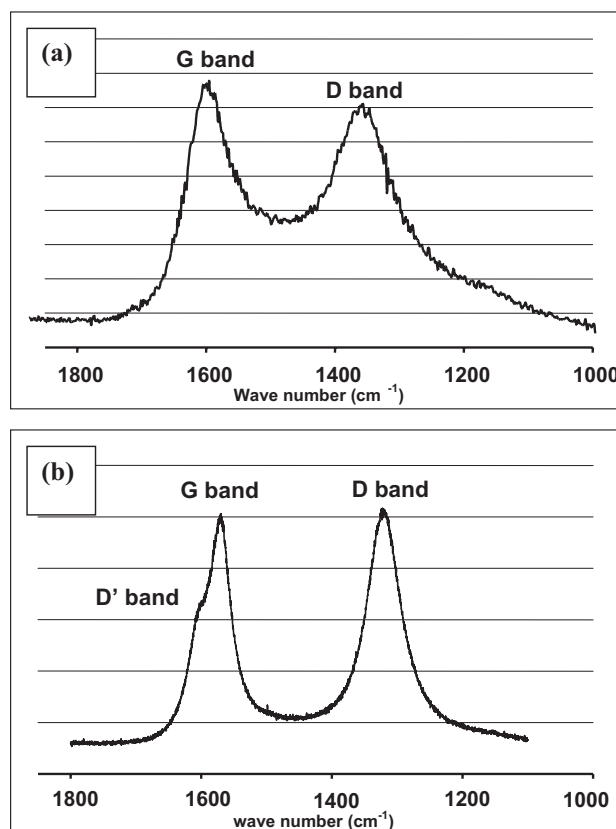


Fig. 7. Raman spectra of a) GNFs and b) MWCNTs.

ent kinetics of carbon diffusion and precipitation phenomena, occurring at high temperatures and giving rise to the encapsulation of active particles.

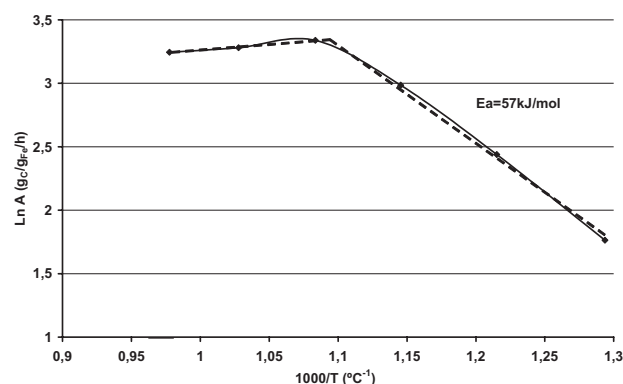
As for GNF growth, we also observe for MWCNTs an increase in the bed height which is proportional to the pro-

Table 3. Operating conditions used for Fe/Al<sub>2</sub>O<sub>3</sub> catalysts.

Run	Reactor diameter [cm]	Run duration [min]	Mass of catalyst [g]	T [°C]	Q <sub>C<sub>2</sub>H<sub>4</sub></sub> [sccm]	Q <sub>N<sub>2</sub></sub> [sccm]	Q <sub>H<sub>2</sub></sub> [sccm]	(U/U <sub>mi</sub> ) <sub>t=0</sub>
2-1				500				1.06
2-2				550				1.13
2-3				600				1.20
2-4	2.5	60	0.5	650	60	160	120	1.26
2-5				700				1.33
2-6				750				1.40
5-1	5	120	20	650	405	685	1200	0.9
16-1								
16.2	16	120	200	650	11300	6500	3800	0.93

 Table 4. Results obtained for Fe/Al<sub>2</sub>O<sub>3</sub> catalysts.

Run	T [°C]	CNT produced [g]	Final fixed bed height [cm]	Ethylene Conversion [%]	X [gC/g <sub>cata</sub> ]	A [gC/g <sub>M</sub> h <sup>-1</sup> ]
2-1	500	0.28	~0.45	7.8	0.56	5.83
2-2	550	0.55	0.65	15.3	1.10	11.46
2-3	600	0.95	1.3	26.4	1.90	19.79
2-4	650	1.35	1.9	37.6	2.70	28.17
2-5	700	1.28	1.5	35.5	2.55	26.60
2-6	750	1.23	1.5	34.2	2.46	25.65
5-1	650	40.4	36.1	83.2	2	9
16-1	650	535	40	39.5	2.7	13.9
16-2	650	551	38	40.7	2.75	14.3


 Fig. 8. Arrhenius plot for activation energy of MWCNTs grown on Fe/Al<sub>2</sub>O<sub>3</sub> catalysts.

ductivity, but for this latter case, it is more significant and more spectacular. Thus, at 650 °C, where the best productivity is achieved, the bed height is approximately nineteen times more significant than the initial height. SEM analysis (Fig. 9) shows a huge coverage with a globular mass of MWCNTs and a significant increase in the diameter of the catalytic grains. As for Ni, it results from the explosion of the composite grains, accompanied by a significant decrease in the apparent density. A description of how the catalyst operates is discussed elsewhere.<sup>[24,34]</sup> Briefly, like a nickel catalyst, the catalytic grains explode quite rapidly during the MWCNT growth due to reaction in the macro-

and mesopores of the support, leading to a further growth all over the formed pieces, and expansion of the total bed volume.

Contrary to the Ni/Al<sub>2</sub>O<sub>3</sub> catalyst, there is no significant effect of temperature on the diameter of the MWCNTs. We can see on the TEM images (Fig. 10) that the production is homogeneous with external diameters in the range 10–20 nm. At 550 °C, we can observe a filamentous carbon by-product due to large catalyst particles. The absence of these large particles at temperatures above 550 °C indicates that a restructuring of the catalyst is occurring at higher temperatures. Metal dusting is a carburization phenomenon which proceeds at 400–800 °C in strongly carburizing atmospheres,<sup>[41]</sup> and this phenomenon could be the origin of large particles disintegrating into smaller ones at temperatures above 550 °C. Moreover, iron particle fragmentation during carbon filament growth was reported more than thirty years ago by Baker et al.<sup>[35]</sup> Finally, the Raman spectra of the purified nanotubes produced at 650 °C (Fig. 7b) is consistent with graphitic MWCNTs.<sup>[42]</sup> It shows the G and D characteristic bands of graphite material and disordered carbon, respectively. The I<sub>D</sub>/I<sub>G</sub> ratio is 1.02. The G band presents a shoulder, D', assigned to a double resonance of the D band.<sup>[42]</sup> TGA measurements conducted on these purified MWCNTs indicate a mass loss of 98.5 % (1.5 % of remaining iron), while BET measurements show a surface area of 327 m<sup>2</sup> g<sup>-1</sup> with a corresponding pore volume of 0.96 mL g<sup>-1</sup>.

The selective preparation of GNFs (Ni/Al<sub>2</sub>O<sub>3</sub> catalyst) and MWCNTs (Fe/Al<sub>2</sub>O<sub>3</sub> catalyst) by FB-CCVD in a small diameter quartz reactor has been achieved. However, with such a reactor, the fluidization quality cannot be optimal due to wall effects and to the poor efficiency of the gas distributor (fritted quartz plate). Thus, we decided to study, in the case of the Fe/Al<sub>2</sub>O<sub>3</sub> catalysts, the synthesis of MWCNTs in larger diameter FB-CVD reactors with internal diameters of 5.3 and 16 cm (Fig. 11).

The selective preparation of GNFs (Ni/Al<sub>2</sub>O<sub>3</sub> catalyst) and MWCNTs (Fe/Al<sub>2</sub>O<sub>3</sub> catalyst) by FB-CCVD in a small diameter quartz reactor has been achieved. However, with such a reactor, the fluidization quality cannot be optimal due to wall effects and to the poor efficiency of the gas distributor (fritted quartz plate). Thus, we decided to study, in the case of the Fe/Al<sub>2</sub>O<sub>3</sub> catalysts, the synthesis of MWCNTs in larger diameter FB-CVD reactors with internal diameters of 5.3 and 16 cm (Fig. 11).

## 3.2. Scale-Up Operation

### 3.2.1. MWCNT Production in a 5.3 cm FB Reactor

We discuss here run 5-1 the operating conditions of which are detailed in Table 3. Only 20 g of catalyst has been used to prevent the reactor becoming completely filled by the composite powder. This mass corresponds to an initial fixed-bed height of 0.7 cm. Results are given in Table 4. It is worth noting that a partial agglomeration of the FB occurs during this experiment since the bottom part of the bed, near the entrance of the fresh reactive gases, is not fully fluidized. This results in a decrease of around

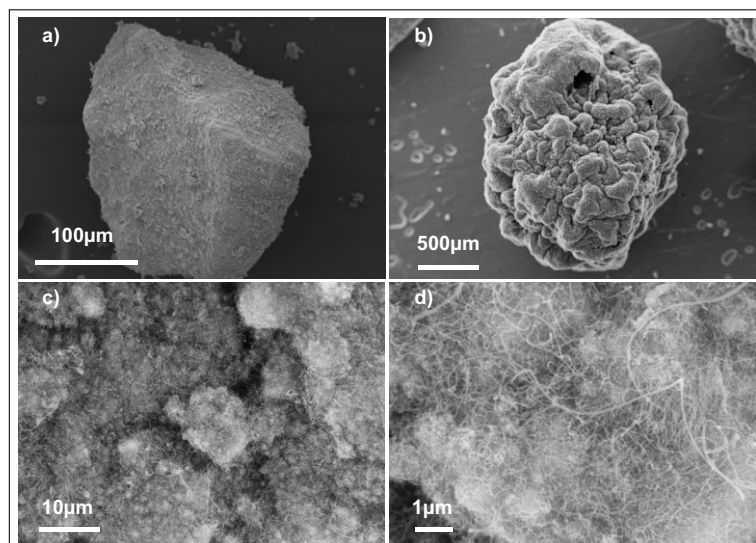


Fig. 9. SEM images of the Fe catalyst and the composite powder obtained at 650 °C: a) original Fe/Al<sub>2</sub>O<sub>3</sub> catalyst, and b-d), composite powder.

80 °C of the FB temperature 3 cm above the distributor, 30 min after the beginning of the run. These phenomena probably lower the carbon conversion and catalyst efficiency. They are clearly due to the high activity of this 10% Fe/Al<sub>2</sub>O<sub>3</sub> catalyst since, for similar operating conditions in the same FB reactor, they do not occur when using less efficient 2.5% Fe/Al<sub>2</sub>O<sub>3</sub> catalysts, as detailed elsewhere.<sup>[34]</sup>

This local agglomeration probably proceeds from an intense growth of CNT agglomerates around the catalyst grains.

As in the FB reactor of 2.5 cm, an impressive expansion of the bed occurs, since the final fixed-bed height corresponds to more than 50 times the initial one. The reason is the same as that proposed previously: the grain density of the materials decreases with time and simultaneously the grains explode due to the CNT growth inside the pores of the catalyst.<sup>[34]</sup> Thus, the apparent grain density varies from 1810 kg m<sup>-3</sup> for the initial catalytic powder to 90 kg m<sup>-3</sup> for the final composite powder. Thanks to this high bed expansion, the carbon conversion is quite satisfactory (>83%) and higher than that obtained in the 2.5 cm reactor. This can be explained by the fact that the residence time of the reactive gases is directly proportional to the bed height for similar gas velocities, and is thus higher here. Even if the operating conditions are not strictly identical, the

40 g of CNT formed can be compared to the 1.3 g of CNT synthesized in the 2.5 cm FB reactor: the scale factor is quite reasonable since we have used here a mass of catalyst 40 times higher than in the small reactor. The productivity *X* and activity *A* are slightly lower than in the 2.5 cm reactor because the amount of carbon arriving per gram of catalyst is lower here than in the small contactor.

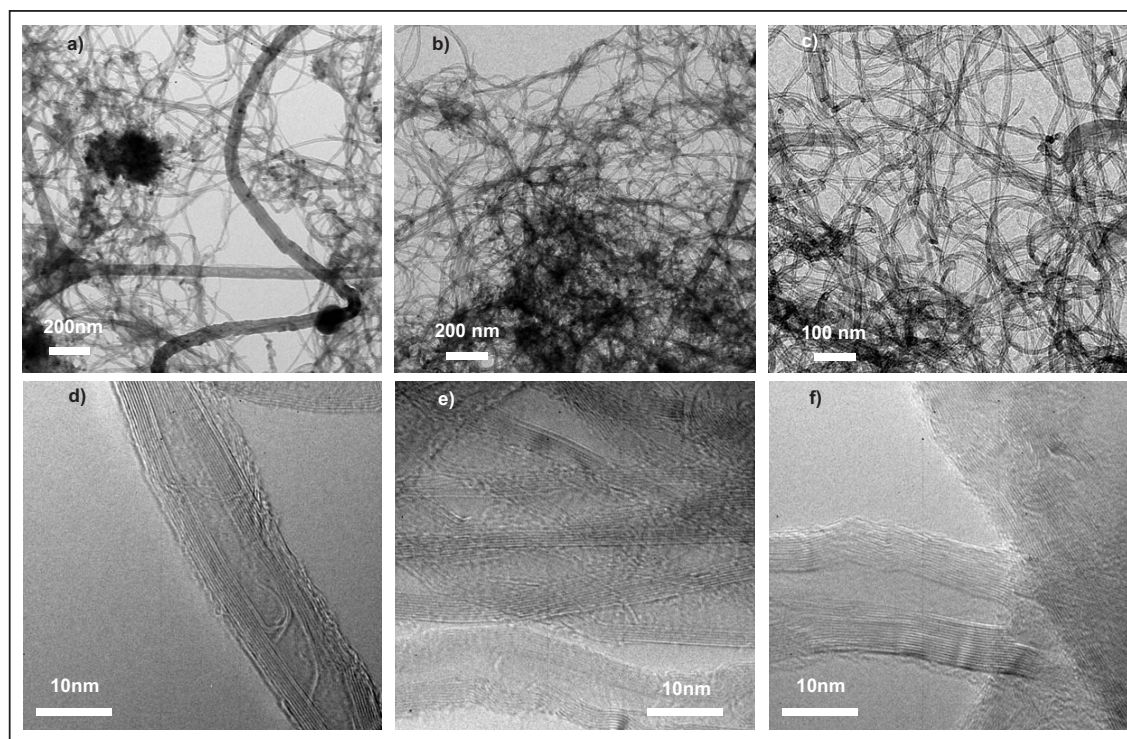


Fig. 10. TEM images of MWCNTs grown at a) and d) 550 °C, b) and e) 650 °C, and c) and f) 750 °C.



Fig. 11. Photographs of the 5.3 cm i.d. and the 16 cm i.d. FB-CVD reactors.

TGA measurements, TEM observations, and Raman spectroscopy have been used to characterize the purified product, and have proved the complete selectivity of the process. The structural features of the CNTs formed are identical to those obtained in the 2.5 cm FB reactor.

### 3.2.2. MWCNT Production in a 16 cm Diameter FB Reactor

Two reproducibility experiments have been performed corresponding to runs 16-1 and 16-2 of Table 3. The inlet molar fraction of ethylene is three times higher than for run 5-1 whereas the fluidization ratio and run duration are similar. An amount of 200 g of catalyst has been used leading to an initial fixed-bed height of 1.2 cm. Results are given in Table 4. First, no agglomeration at all occurs during these experiments. As in the other FB reactors, an impressive bed expansion takes place, since the final fixed-bed height corresponds to more than 30 times the initial one. We observe that the bed expansion is, as expected, lower than in the 5 cm FB reactor since the surface area of the column is higher, the apparent grain density at the end of the runs being similar to that obtained previously, i.e., around  $90 \text{ kg m}^{-3}$ .

The carbon conversion is logically lower than in the 5 cm reactor since the residence time of the reactive gases is smaller, and the inlet molar fraction of ethylene is higher. The scale-up of the process is particularly efficient regarding the mass of CNTs produced: using a mass of catalyst 10 times higher than in the 5 cm reactor, the mass of CNTs is more than 13 times higher in the 16 cm contactor. This positive result is obtained since the productivity  $X$  and the activity  $A$  are higher than in the 5 cm reactor, because the interphase contact between gas and solids is obviously improved in the 16 cm reactor. In-

deed, wall effects are less important, bubble diameters are smaller, and slugging phenomena are less intense when the bed diameter is higher and the ratio between the fixed-bed height and the reactor diameter is lower.<sup>[4]</sup> This leads to higher heat and mass transfer rates. A consequence and a proof of this improved interphase contact lies in the fact that no agglomeration occurs. Thus, with this laboratory pilot-scale equipment (Fig. 11), the production rate of MWCNTs exceeds  $260 \text{ g h}^{-1}$ , a value which is significant for an academic laboratory given present international research in this area.

Once again, TGA measurements prove the total selectivity of the process, even at this pilot-scale level. The structural features of the purified CNTs are identical to those obtained in the other FB reactors. Figure 12 shows a photograph and micrographs of purified MWCNTs produced in the 16 cm i.d. reactor.

## 4. Experimental

**Catalyst Preparation:** The two  $\text{Ni}/\text{Al}_2\text{O}_3$  and  $\text{Fe}/\text{Al}_2\text{O}_3$  catalysts used in this research were prepared by FB-(OM)CVD in a specially designed vessel described elsewhere<sup>[43]</sup> from alumina ( $204 \text{ m}^2 \text{ g}^{-1}$ ,  $d_{v,50} = 301 \mu\text{m}$ ,  $U_{mf} = 3.1 \text{ cm s}^{-1}$ ) and nickelocene in the presence of hydrogen, and iron pentacarbonyl in the presence of water vapor. These co-reactants were used in order to assist the decomposition of each precursor in the corresponding metal. The solid nickelocene precursor was sublimed at  $110^\circ\text{C}$ , the liquid pentacarbonyl iron precursor was evaporated at  $50^\circ\text{C}$ , and the two were decomposed in the fluidized bed of alumina at  $220^\circ\text{C}$  using nitrogen as the vector gas. The pressure in the reactor was kept at 50 Torr. The metal loading, determined by inductively coupled plasma (ICP), was found to be of 8.4% (w/w) for the  $\text{Ni}/\text{Al}_2\text{O}_3$  catalyst and 9.6% (w/w) for the  $\text{Fe}/\text{Al}_2\text{O}_3$  catalyst.

**GNF and CNT Production in the 2.5 cm Quartz Reactor:** Experiments were carried out in a conventional vertical quartz CVD reactor of 2.5 cm i. d. and 20 cm height, heated with an electric furnace. The gas distributor was a porous quartz plate. GNFs or MWCNTs were synthesized by CCVD on

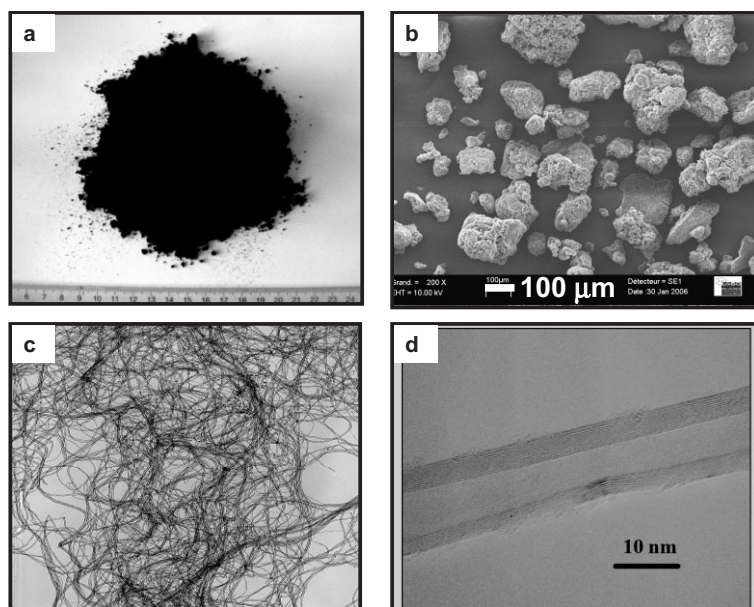


Fig. 12. a) Photograph, b) SEM image, and c), d) TEM images of purified MWCNTs powder.

0.5 g of Ni/Al<sub>2</sub>O<sub>3</sub> or Fe/Al<sub>2</sub>O<sub>3</sub> catalyst, respectively, (initial bed height lower than 1 mm). For each catalyst, all the experimental conditions except the temperature were kept fixed in order to investigate the effects of temperature on the catalytic performances, and on the nature of the products. The studied temperature range was 400–750 °C for GNF synthesis, and 550–750 °C for MWCNT synthesis.

**MWCNT Production in the 5 cm and 16 cm Diameter Reactors:** The FB reactors were entirely constructed in 304L stainless steel; their dimensions being 5.3 cm i.d. and 1 m height, and 16 cm i.d. and 1 m height, respectively. A photograph of these FB reactors is provided in Figure 11. For both reactors, the gas distributor was a stainless steel perforated plate covered with a stainless steel grid supplied with 50 µm holes. In each case, a multi-zone electric furnace allowed monitoring of the FB temperature via several thermocouples fixed on the outer reactor wall. Temperatures at various levels inside the FB were registered through thermocouples placed along the reactor axis.

Electronic grade ethylene, hydrogen, and nitrogen gases (Air Liquide) were supplied to the reactors through mass flow meters. For the two reactors, a pressure sensor allowed measuring the differential pressure drop between the bottom and the top parts of the reactors. After their exit from the reactors, the gaseous effluents flowed through a bag filter, in order to collect eluted particles or fines that could be formed during experiments. The catalyst is a 9.6 % Fe/Al<sub>2</sub>O<sub>3</sub> powder synthesized as described in Section 4.1.

**Operating Protocol:** First a controlled mass of catalyst was introduced into the reactor. A constant flow rate of a mixture of nitrogen and hydrogen was maintained to fluidize the bed during its heating, the initial fluidization ratio  $U/U_{mf}$ , where  $U$  is the superficial gas flow velocity and  $U_{mf}$  the minimum fluidization velocity, being most often fixed at about 1. As soon as the thermal regime was reached, the flow rate of nitrogen was lowered to a pre-calculated value and, simultaneously, ethylene was introduced into the bed to maintain a constant total flow rate. It is worth noting that, during the synthesis of CNTs,  $U_{mf}$  decreased with run duration, since the grain density sharply decreased. As a consequence, the fluidization ratio increased with run duration. This explains why the initial fluidization ratio was fixed at a minimal value.

**Characterization of the Carbon Deposits:** After each run, the fixed-bed height was measured; the carbon deposit was weighed and submitted to TGA, SEM, and TEM. TGA measurements were conducted on a Setaram thermobalance in which the sample was heated in air from 25 to 1000 °C at a rate of 10 °C min<sup>-1</sup>, followed by a 30 min isotherm. The TEM images were obtained using a Philips CM12 microscope operating at 120 kV. The SEM observations were performed using a field-enhanced electron microscope (Hitachi S-4500 I) and a LEO 435 microscope. Raman spectra were recorded on a Labram HR800 from Jobin et Yvon (632.82 cm<sup>-1</sup>). The distribution of grain diameters in volume was measured with a Mastersizer Sirocco 2000 laser granulometer. CNT purification was performed by H<sub>2</sub>SO<sub>4</sub> washing in order to remove the catalyst.

Received: October 30, 2006

Revised: March 9, 2007

- [1] M. Monthieux, P. Serp, E. Flahaut, C. Laurent, A. Peigney, M. Razafimanana, W. Bacsá, J.-M. Broto in *Springer Handbook of Nanotechnology* 2nd ed., (Ed: B. Bhushan), Springer-Verlag, Heidelberg, Germany, 2007.
- [2] M. L. Terranova, V. Sessa, M. Rossi, *Chem. Vap. Deposition* **2006**, *12*, 315.
- [3] E. Couteau, K. Hernadi, J. W. Seo, L. Thien-Nga, C. Miko, R. Gaal, L. Forro, *Chem. Phys. Lett.* **2003**, *378*, 9.
- [4] D. Kunii, O. Levenspiel, *Fluidization Engineering 2nd Edition*, Butterworth-Heinemann, Oxford 1991.
- [5] T. Xie, K. B. McAuley, J. C. C. Hsu, D. W. Bacon, *Ind. Eng. Chem. Res.* **1994**, *33*, 449.
- [6] D. Venegoni, P. Serp, R. Feurer, Y. Kihn, C. Vahlas, P. Kalck, *Carbon* **2002**, *40*, 1799.
- [7] B. C. Liu, L. Z. Gao, Q. Liang, S. H. Tang, M. Z. Qu, Z. L. Yu, *Catal. Lett.* **2001**, *71*, 225.
- [8] M. A. Ermakova, D. Y. Ermakov, G. G. Kuvnishov, L. M. Plyasova, *J. Catal.* **1999**, *187*, 77.
- [9] S. M. Bachilo, L. Balzano, J. E. Herrera, F. Pompeo, D. E. Resasco, B. Weisman, *J. Am. Chem. Soc.* **2003**, *125*, 11186.
- [10] G. G. Kuvnishov, Y. I. Mogilnykh, D. G. Kuvnishov, M. A. Ermakova, D. Y. Ermakov, A. N. Salanov, N. A. Rudina, *Carbon* **1999**, *37*, 1239.
- [11] A. Weidenkaff, S. G. Ebbinghaus, P. Mauron, A. Reller, Y. Zhang, A. Züttel, *Mater. Sci. Eng. C* **2002**, *19*, 119.
- [12] P. Mauron, C. Emmenegger, P. Sudan, P. Wenger, S. Rentsch, A. Züttel, *Diamond Relat. Mater.* **2003**, *12*, 780.
- [13] B. C. Liu, L. Z. Gao, Q. Liang, S. H. Tang, M. Z. Qu, Z. L. Yu, *Chin. J. Chem.* **2001**, *19*, 983.
- [14] H. Li, S. H. Tang, L. Z. Gao, B. C. Liu, Q. Liang, B. Zhang, Z. L. Yu, *J. Nat. Gas Chem.* **2001**, *10*, 203.
- [15] M. A. Ermakova, D. Y. Ermakov, A. L. Chuvilin, G. G. Kuvnishov, *J. Catal.* **2001**, *201*, 183.
- [16] M. Perez-Cabero, I. Rodriguez-Ramos, A. Guerrero-Ruiz, *J. Catal.* **2003**, *215*, 316.
- [17] W. Qian, F. Wei, T. Liu, Z. W. Wang, H. Yu, G. Luo, L. Xiang, X. Deng, *AIChE J.* **2003**, *49*, 619.
- [18] Y. L. Li, I. A. Kinloch, M. S. P. Shaffer, J. Geng, B. Jhonson, A. H. Windle, *Chem. Phys. Lett.* **2004**, *384*, 98.
- [19] M. A. Ermakova, D. Y. Ermakov, G. G. Kuvnishov, *Appl. Catal. A* **2000**, *201*, 61.
- [20] Y. Wang, F. Wei, G. Gu, H. Yu, *Physica B* **2002**, *323*, 327.
- [21] W. Qian, H. Yu, F. Wei, Q. Zhang, Z. Zhang, *Carbon* **2002**, *40*, 2961.
- [22] W. Qian, L. Tang, W. Zhanwen, W. Fei, L. Zhifei, L. Guohua, L. Yongdan, *Appl. Catal. A* **2004**, *260*, 223.
- [23] Y. Wang, F. Wei, G. Luo, H. Yu, G. Gu, *Chem. Phys. Lett.* **2002**, *364*, 568.
- [24] M. Corrias, B. Caussat, A. Ayrál, J. Durand, Y. Kihn, Ph. Kalck, Ph. Serp, *Chem. Eng. Sci.* **2003**, *58*, 4475.
- [25] A. Jess, C. Kern, K. Schrögel, A. Jung, W. Schütz, *Chem. Ing. Tech.* **2006**, *78*, 94.
- [26] J. X. Liu, Z. Ren, L. Y. Duan, Y. C. Xie, *Coll. Chem. Mol. Eng.* **2004**, *62*, 775.
- [27] Q. Wang, G. Ning, F. Wei, G. Luo, *Mater. Res. Soc. Sym. Proc.* **2004**, *785*, 313.
- [28] Y. Wang, P. P. Tang, X. M. Wu, G. D. Lin, H. B. Zhang, *Yingyong Huaxue* **2005**, *22*, 117.
- [29] F. Chen, X. B. Zhang, Y. L. Sun, J. P. Cheng, Y. Li, *Wuji Cailiao Xuebao* **2004**, *19*, 931.
- [30] Q. X. Liu, Y. Fang, *Spectrochim. Acta, Part A* **2006**, *64*, 296.
- [31] U. Arena, M. L. Mastellone, G. Camino, E. Boccaleri, *Polym. Degrad. Stab.* **2006**, *91*, 763.
- [32] C. Vahlas, B. Caussat, P. Serp, G. Angelopoulos, *Mater. Sci. Eng. Rep.* **2006**, *53*, 1.
- [33] Y. Hao, Z. Qunfeng, F. Wei, Q. Weizhong, L. Guohua, *Carbon* **2003**, *41*, 2855.
- [34] A. Morançais, B. Caussat, Y. Khin, Ph. Kalck, P. Gaillard, D. Bernard, P. Serp, *Carbon* **2007**, *45*, 624.
- [35] R. T. K. Baker, P. S. Harris, R. B. Thomas, R. J. Waite, *J. Catal.* **1973**, *30*, 86.
- [36] L. Piao, Y. Li, J. Chen, L. Chang, J. Y. S. Lin, *Catal. Today* **2002**, *74*, 145.
- [37] D. Chen, K. O. Christensen, E. Ochoa-Fernandez, Z. Yu, B. Totdal, N. Latorre, A. Monon, A. Holmen, *J. Catal.* **2005**, *229*, 82.
- [38] J. I. Villacampa, C. Royo, E. Romeo, J. A. Montoya, P. Del Angel, A. Monzon, *Appl. Catal. A* **2003**, *252*, 363.
- [39] Y. L. Li, I. A. Kinloch, M. S. P. Shaffer, C. Singh, J. Geng, B. F. G. Johnson, A. H. Windle, *Chem. Mater.* **2004**, *16*, 5637.
- [40] Y. Wang, S. Serrano, J. J. Santiago-Aviles, *Synth. Met.* **2003**, *138*, 423.
- [41] W. T. Tsai, *Mater. Chem. Phys.* **2003**, *82*, 929.
- [42] E. F. Antunes, A. O. Lobo, E. J. Corat, V. J. Trava-Airoldi, A. A. Martin, C. Verissimo, *Carbon* **2006**, *44*, 2202.
- [43] P. Serp, R. Feurer, R. Morancho, P. Kalck, *J. Catal.* **1995**, *157*, 294.